Ordered structure in block polymer solutions: 6. Possible non-equilibrium effects on growth of self-assembling structures

Keiji Mori*, Hirokazu Hasegawa and Takeji Hashimoto†
Department of Polymer Chemistry, Kyoto University, Kyoto 606, Japan
(Received 6 November 1989; accepted 14 November 1989)

We explore non-equilibrium effects on the growth of microdomain structures in block polymer solutions with a neutrally good solvent. The growth of microdomain structures induced by increasing segregation power with increase of polymer concentration ϕ_p is hindered by morphology-dependent non-equilibrium effects. For spherical microdomains with discontinuous interfaces, the effects set in when the change in number of block chains per domain cannot follow the change of ϕ_p. For other types of microdomains with continuous interfaces, such as cylindrical, bicontinuous and lamellar microdomains, the effects set in when the average separation of chemical junctions of block polymer chains along the interface cannot follow the change of ϕ_p. The effects for spheres are primarily caused by 'suppressed mutual diffusivity' of the block chains from one sphere to others with increasing ϕ_p. The effects for other morphologies are caused by 'grain-boundary effects' discussed in the text and/or vitrification of one type of domain. In the case when changes of the states of the system are sufficiently slow, vitrification becomes the primary cause of the non-equilibrium phenomena, regardless of the morphology of the solution.

(Keywords: block polymer; microdomain; non-equilibrium effects; vitrification, grain boundary)

INTRODUCTION

In this series of papers we explore order–disorder transitions and microdomains as self-assembling mechanisms and structures of block polymer solutions[1–5]. In the ordered state, block polymer solutions were found to form various microdomains, such as spherical[1,2,5], cylindrical and lamellar microdomains[3–5], with long-range spatial order. The domain size and interdomain distance D were explored as functions of molecular weight and composition f of the block polymers as well as of temperature T and polymer volume fraction ϕ_p in the solution[1–5].

It was found[5] that spherical domains with discontinuous interfaces are very far from thermal equilibrium, while cylindrical and lamellar microdomains with essentially continuous interfaces are very close to thermal equilibrium.

For morphologies with continuous interfaces, thermal equilibrium was found to be attained at relatively low ϕ_p and high T ('equilibrium regime') but not at higher ϕ_p and lower T ('non-equilibrium regime'). In this paper we will investigate possible sources giving rise to non-equilibrium effects, such as (i) vitrification of one type of domain with higher glass transition temperature T_g, (ii) the effect of grain-boundary relaxation for the morphology of continuous interfaces and (iii) the effect of suppressed mutual diffusivity, especially important for spherical microdomains with discontinuous interfaces.

* Present address: Research Center, Toyobo Co. Ltd, Katata, Ohtsu, Shiga 520-02, Japan
† To whom correspondence should be addressed

0032-3861/90/122368-09

EXPERIMENTAL METHODS

Samples

Diblock polymers of poly(styrene-*b*-isoprene) (SI) were prepared by sequential living anionic polymerization. *Table 1* summarizes the characteristics of the samples used in this study. Number-average molecular weight M_n was characterized by membrane osmometry, M_w/M_n by size exclusion chromatography, composition by elemental analysis, and morphology in bulk by transmission electron microscopy on ultrathin sections of the as-cast films stained by osmium tetraoxide. Toluene is used as the casting solvent.

Small-angle X-ray scattering

Microdomain structures in solutions were investigated as a function of ϕ_p by *in situ* small-angle X-ray scattering (SAXS), as reported and discussed previously[3].

Differential scanning calorimetry

Glass transition temperatures of toluene solutions of homopolystyrene (HK-11) and a particular SI (HY-10) were measured as a function of ϕ_p by d.s.c. (Perkin–Elmer, DSC-2C). Toluene solutions with given ϕ_p values were first prepared and subsequently enclosed in pans for the d.s.c. measurements. A small amount of toluene evaporated during the d.s.c. experiments, which caused an increase of polymer concentration by about 2% on average. The change of concentration was measured by weighing the empty pan and the pan containing a given solution before and after the measurement.

Table 1 Sample characteristics

Specimen	$M_n \times 10^{-4}$	PS/PI (wt%/wt%)	M_w/M_n	Morphology in bulk
L-8	9.4	50/50	–	Alternating lamellae
HS-10	8.1	63/37	1.13	Alternating lamellae
C-1	8.6	33/67	–	PS cylinders in a PI matrix
HY-10	16.4	69/31	1.17	'Tetrapod' network
S-4	22.0	85/15	–	PI spheres in a PS matrix
HK-11	8.7	100/0	–	–

EXPERIMENTAL RESULTS

SAXS results

SAXS profiles for toluene solutions of the block polymers were measured *in situ* as a function of concentrations at room temperature[3].

The solutions of the block polymers L-8 and HS-10 showed SAXS profiles[3,4] relevant to alternating lamellar microdomains, i.e. multiple-order scattering maxima at peak positions that were integer multiples of the first-order peak position. It should be noted here that some of the higher-order maxima may be suppressed relative to others depending on the volume fraction of one type of lamella. From the peak position we can determine the interdomain distance (or lamellar identity period) D with high accuracy. Typical SAXS profiles will be found in our previous papers[3,4].

The solutions of block polymers C-1 and HY-10 showed SAXS profiles relevant to cylindrical microdomains with long-range spatial order, i.e. with two-dimensional hexagonal arrays. The profiles exhibited multiple-order scattering maxima (shown by thin arrows) at peak positions of 1 and $\sqrt{3}$ relative to the first-order peak, as well as broad maxima (shown by thick arrows) arising from isolated cylinders (see *Figure 1*). Although HY-10 in bulk showed the bicontinuous tetrapod-network structure[6] equivalent to the double diamond lattice[7], its SAXS profile was shown to be almost identical to that for hexagonally packed cylinders. This was interpreted as a consequence of the extra peaks[7], which may appear at peak positions of $\sqrt{3/2}$ and $\sqrt{2}$ between 1 and $\sqrt{3}$ relative to the first-order peak, not being resolvable because they are so closely spaced for this particular specimen. The solutions of HY-10 also show SAXS profiles relevant to cylindrical domains with long-range spatial order. From the peak positions arising from interdomain interference, one can determine the intercylinder distance D with high accuracy:

$$D = \sqrt{4/3}\, D_s \tag{1}$$

where D_s is the Bragg spacing as measured from the first-order scattering maximum:

$$2D_s \sin\theta_{hk0} = (h^2 + hk + k^2)^{1/2}\lambda, \qquad (h, k = \text{integers}) \tag{2}$$

Here $2\theta_{hk0}$ are the scattering maxima and λ is the X-ray wavelength.

The block polymer solutions S-4 show spherical microdomains with long-range spatial order and multiple-order scattering maxima at positions $1:\sqrt{2}:\sqrt{3}$, etc., and broad scattering maxima arising from isolated spheres[5]. From the scattering maxima arising from intersphere interference, one can estimate the Bragg spacing D_s, and from the maxima arising from isolated spheres, one can estimate the average radius of the spheres R_s (ref. 5).

Figure 2 shows the interdomain distances D for lamellar microdomains (L-8 and HS-10) and for cylindrical microdomains (C-1 and HY-10) as functions of ϕ_p. The figure also includes the vertical shaded zone where vitrification of the PS microdomains takes place, as will be discussed later. *Figure 3* shows the change of D_s and R_s for spherical microdomains of S-4 as a function of ϕ_p.

It is clearly seen that D in *Figure 2* scales with ϕ_p:

$$D \sim \phi_p^{1/3} \qquad \text{for } \phi_p < \phi_{T_g} \tag{3}$$

where the system attains thermal equilibrium at a given timescale of observation, and ϕ_{T_g} is the vitrification concentration ϕ_p at which the glass transition temperature of PS microdomains reaches room temperature, i.e. ambient temperature for microdomain formation. The deviation from the straight line in the double-logarithmic plot (equation (3)) occurs at $\phi_p \gtrsim \phi_{T_g}$ and is believed to reflect the non-equilibrium effects on domain growth, as will be discussed later. The growth of the domains with increasing ϕ_p in the equilibrium regime is a consequence of increasing segregation power with ϕ_p (refs. 3, 4). Here the segregation effect much outweighs the effect of decreasing chain dimensions due to decreased chain expansion coefficient with increasing ϕ_p. The latter effect, of course, tends to decrease D in order to satisfy the incompressibility requirement[3,4]. For some polymers, e.g. L-8 and HY-10, the non-equilibrium effect seems to set in earlier than the non-equilibrium effect involved by vitrification, viz. at ϕ_p lower than ϕ_{T_g}, a possible interpretation of which will be given later.

In contrast to lamellar and cylindrical domains, spherical domains are observed to encounter the non-equilibrium effect at ϕ_p much lower than ϕ_{T_g}, i.e. $\phi_p \ll \phi_{T_g}$, as seen in *Figure 3*. The broken line for D_s, given by equation (3), indicates the expected concentration dependence of D_s when spherical domains can achieve thermal equilibrium. The chain lines for D_s and R_s, which are given by:

$$D_s, R_s \sim \phi_p^{-1/3} \tag{4}$$

indicate the concentration dependences of D_s and R_s for the non-equilibrium system where the number of block chains N_s per single spherical domain is fixed during the solvent evaporation process. The experimental results on D_s and R_s closely follow the trends expected for the non-equilibrium process, starting at relatively low ϕ_p, i.e. at $\phi_p > \phi_f \simeq 0.3$ for S-4/toluene. The fact that $\phi_f \ll \phi_{T_g}$ will be discussed later.

D.s.c. results

One can think of vitrification of microdomains with

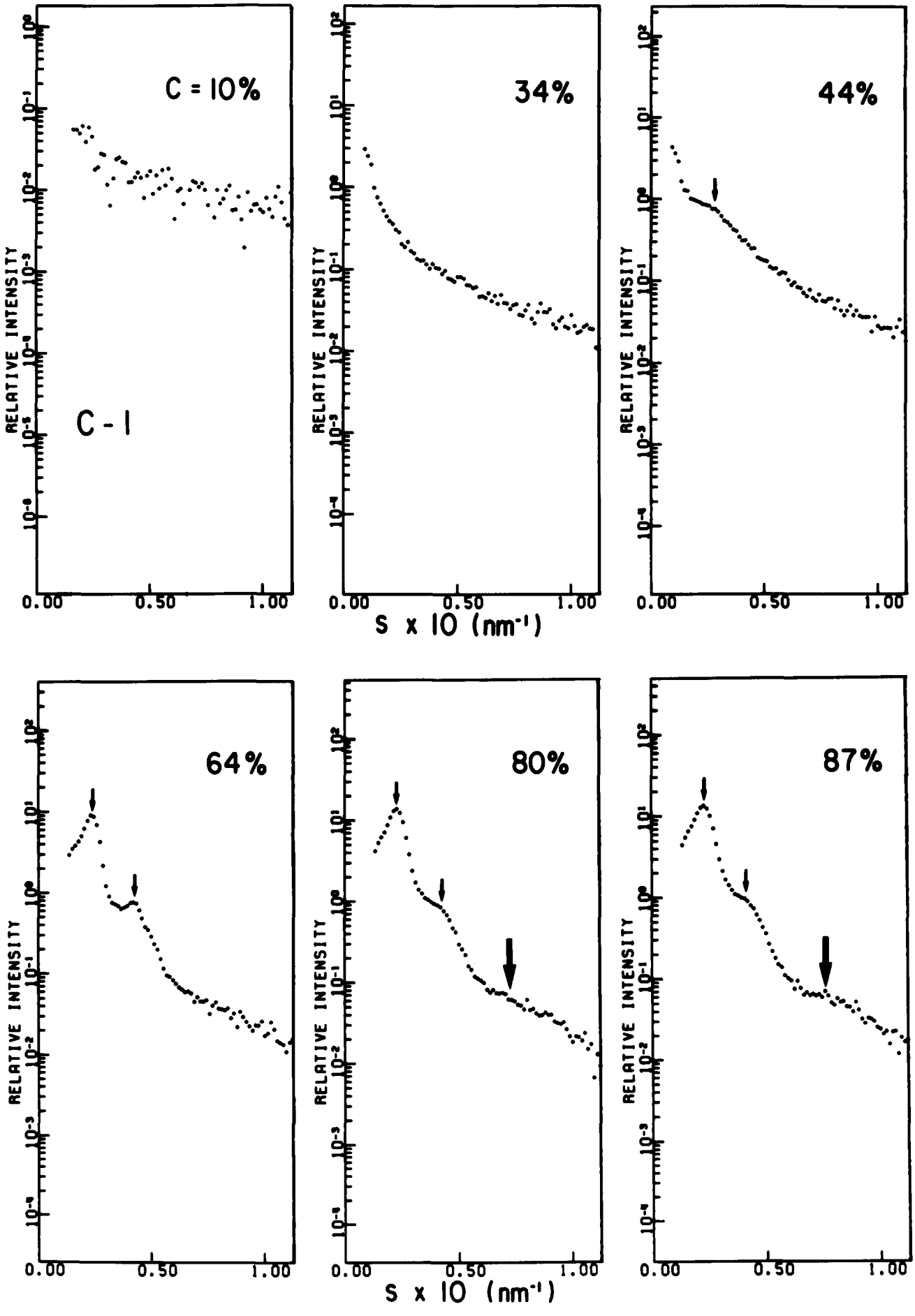

Figure 1 SAXS profiles for toluene solutions of C-1 at $\phi_p = 0.091$, 0.317, 0.414, 0.616, 0.783 and 0.858. All the profiles at higher concentrations ($C \gtrsim 64\%$) show hexagonally packed cylindrical microdomains

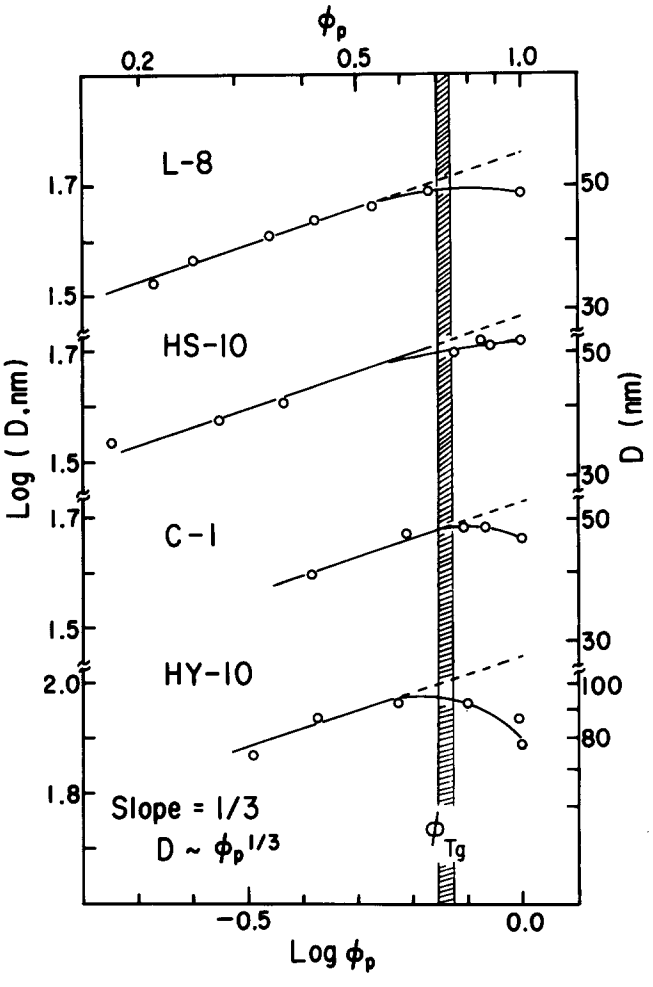

Figure 2 Concentration dependence of domain identity period for lamellar microdomains (L-8 and HS-10) and interdomain distance for cylindrical microdomains (C-1 and HY-10). The vertical shaded zone is the vitrification concentration ϕ_{T_g} at which the glass transition temperature of polystyrene-rich domains becomes room temperature (ambient temperature). Toluene was used as a commonly good solvent for both polystyrene and polyisoprene

higher glass transition temperature T_g as a possible cause of non-equilibrium effects. From this viewpoint, we measured T_g as a function of ϕ_p for the block polymer HY-10 and homopolystyrene HK-11.

Figures 4 and *5* represent the d.s.c. thermograms obtained during cooling cycles at a rate of 5 K min^{-1} for HK-11 and HY-10, respectively, at various polymer concentrations, as indicated in the figures. The glass transition for each solution was assessed at the midpoint where the characteristic change in the thermogram occurs as shown by the arrows. All the solutions studied in *Figure 5* (HY-10 solutions) have microdomains comprising PS-rich solution and PI-rich solution and hence should have two T_g values corresponding to each microphase. However, we studied here only the higher T_g, i.e. the T_g for the polystyrene-rich microphase.

The T_g values thus estimated as a function of ϕ_p are summarized in *Figure 6*, where parts (a) and (b) show the results for HY-10 and HK-11, respectively. The error bars indicate the change of ϕ_p before and after the d.s.c. measurements. The results indicate that the *vitrification concentration* ϕ_{T_g} is 0.7 for HY-10 and 0.75 for HK-11. It is not well understood at present why ϕ_{T_g} for HY-10 is lower than ϕ_{T_g} for HK-11. We expect that mixing of a small amount of polyisoprene block in the polystyrene microdomains tends to lower T_g and hence increase ϕ_{T_g} of the polystyrene domains. Thus mixing caused by the suppressed segregation power due to the solvent is expected to cause ϕ_{T_g} for HY-10 to be slightly higher than ϕ_{T_g} for HK-11, which is in contrast to the experimental results. The experimental results may be interpreted as an effect of molecular weight coupled together with that of local concentration fluctuations of polymer on T_g.

If T_g is assessed as the temperature at which a new baseline is established in the d.s.c. thermogram after completion of the transition, i.e. the lower temperature

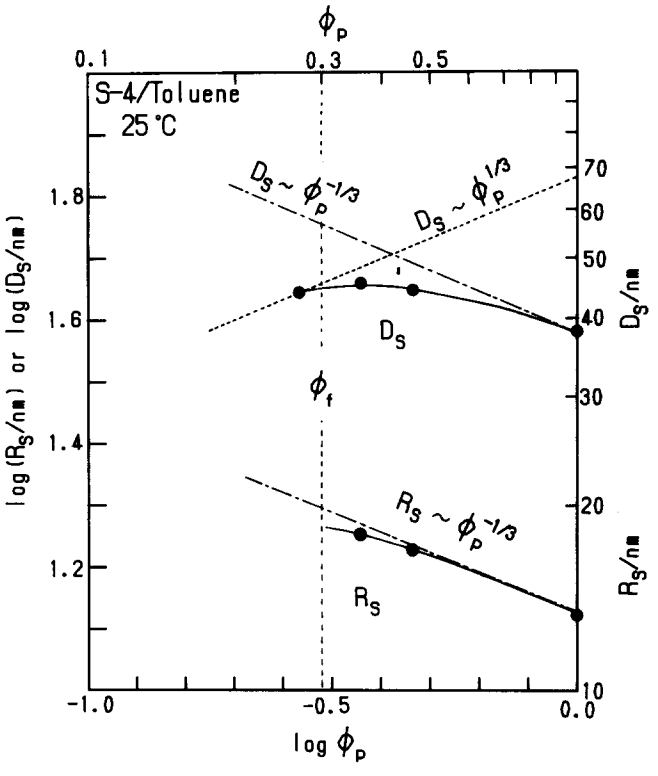

Figure 3 Bragg spacing D_s and radius of spherical microdomains R_s for S-4 as a function of concentration ϕ_p. The observed values for D_s and R_s are shown by filled circles

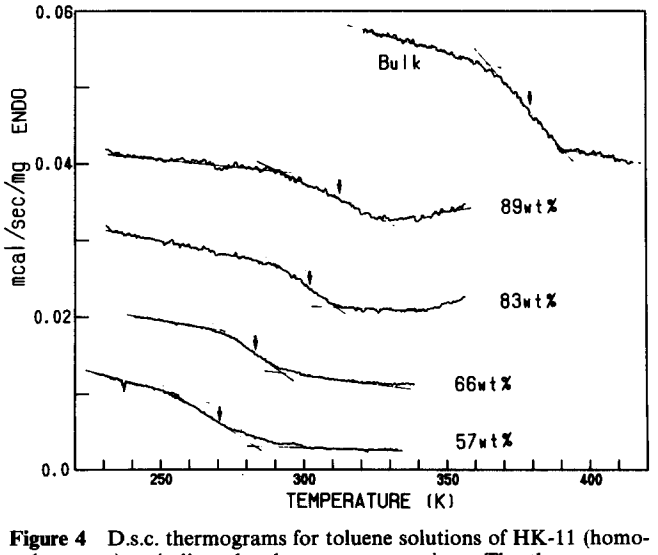

Figure 4 D.s.c. thermograms for toluene solutions of HK-11 (homopolystyrene) at indicated polymer concentrations. The thermograms were obtained during cooling cycles at a rate of 5 K min^{-1}

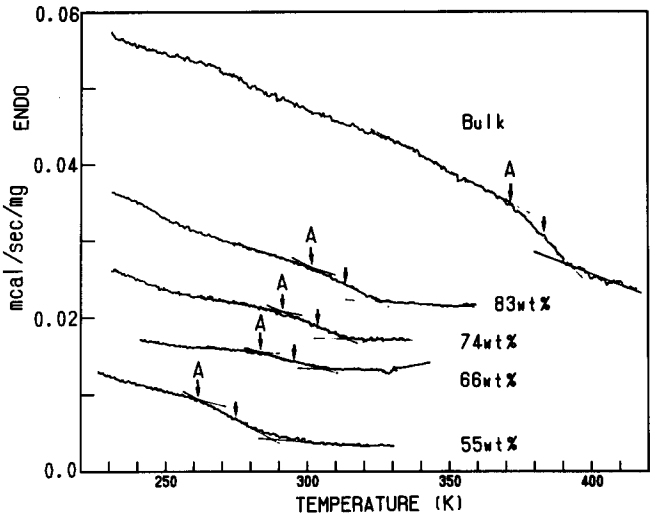

Figure 5 D.s.c. thermograms for toluene solutions of HY-10 (SI block polymer) at indicated polymer concentrations. The thermograms were obtained during cooling cycles at a rate of 5 K min^{-1}. Only the glass transition of polystyrene-rich microdomains was highlighted

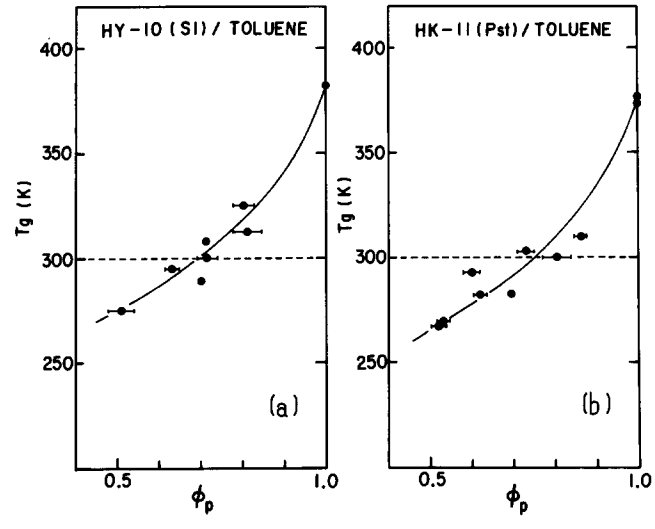

Figure 6 Concentration dependence of glass transition temperature of (a) polystyrene-rich microdomains of HY-10 (SI block polymer) and (b) HK-11 (homopolystyrene)

indicated by point A in *Figure 5* rather than the midpoint shown by the arrow, the T_g values are lower than the T_g values shown in *Figure 6* by $\sim 10°C$, and ϕ_{T_g} becomes higher than ϕ_{T_g} estimated from *Figure 6* by ~ 0.05. Consequently we determined ϕ_{T_g} for the block polymer solutions studied here as:

$$\phi_{T_g} = 0.70 \text{ to } 0.75 \tag{5}$$

for further discussions on the non-equilibrium effect caused by vitrification. This concentration range corresponds to the width of the vertical shaded zone in *Figures 2* and *8*.

DISCUSSION

Equilibrium and non-equilibrium regimes

From simple volumetric considerations, one obtains the following relationships:

$$D = 2(v_A + v_B)N/S \tag{6}$$

for the interdomain distance of lamellae;

$$R_{c,A} = 2v_A N/S \tag{7}$$

for the radius $R_{c,A}$ of an A cylinder; and

$$R_{s,A} = 3v_A N/S \tag{8}$$

for the radius $R_{s,A}$ of an A sphere. Here v_K is the volume occupied by the single K-block polymer chain (K = A or B), and N/S is the number density of chemical junctions, i.e. the number of block polymer chains per unit interfacial area. It is obvious that:

$$v_A, v_B \sim \phi_p^{-1} \tag{9}$$

for the neutral solvent. The domain size in the equilibrium regime follows the scaling law established experimentally[3,4]:

$$D, R_{c,A}, R_{s,A} \sim \phi_p^{1/3} \tag{10}$$

as $R_{c,A} \sim D$ and $R_{s,A} \sim D_s$. Here it should be noted that the scaling law for spherical microdomains suffers from greater uncertainty than those for lamellar and cylindrical microdomains, because of the dominant non-equilibrium effect. However, we assume that the scaling law for spherical domains is the same as those for lamellar and cylindrical domains. From equations (9) and (10) it follows that:

$$N/S \sim \phi_p^{4/3} \tag{11}$$

and

$$N_s \sim \phi_p^2 \tag{12}$$

for the equilibrium regime, where N_s is the number of block chains per single spherical microdomain.

Thus domain growth driven by the increasing segregation power involves an increase of N/S or N_s, i.e. an increase of the interfacial density of the chemical junctions. This increase of N/S is accompanied by a decrease of the average distance a between nearest-neighbour junctions from a_1 to a_2 and by a stretching of A- and B-block chains so that their end-to-end distance in the direction normal to the interface R increases from R_1 to R_2, as shown in *Figure 7*[3,4,8]. The latter chain stretching is necessary to satisfy the demand of incompressibility and causes growth of the domain dimensions D, $R_{c,A}$ and $R_{s,A}$[3,4,8]. The increase of N/S for spherical microdomains inevitably involves an increase of N_s.

The reduction of a from a_1 to a_2 and the increase of R from R_1 to R_2 with increasing ϕ_p cause a loss of conformational entropy as well as a loss of placement entropy, i.e. entropy associated with placing the junctions in the interfacial region, the latter entropy loss being encountered because of the reduction of surface-to-volume ratio S/V of the domains. If this penalty of entropy loss is overcome by the reduction of interfacial energy caused by a decrease of S/V, then domain growth takes place.

If the changes of a and end-to-end distance of polymer coils (hence the change of N/S for lamellar and cylindrical domains and of N_s for spherical microdomains) occur within the timescale of experimental observations, the systems can attain thermal equilibrium. If not, the systems cannot attain thermal equilibrium.

Non-equilibrium process for systems with continuous interfaces

The concentration dependences of N/S are analysed for the lamellar and cylindrical domain systems in *Figure 8*.

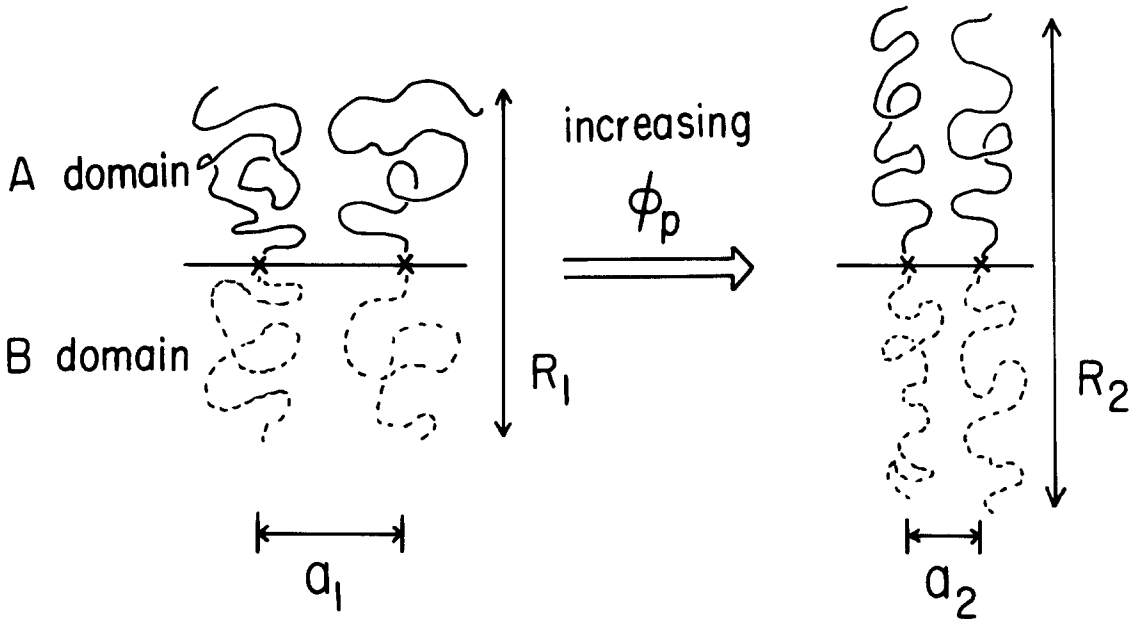

Figure 7 Fundamental molecular processes involved by increasing polymer concentration ϕ_p. Increasing segregation power between PS and PI caused by increasing ϕ_p results in stretching of block chains normal to the interface from R_1 to R_2 and contraction of average interfacial area occupied by a junction point of SI block polymer from a_1^2 to a_2^2

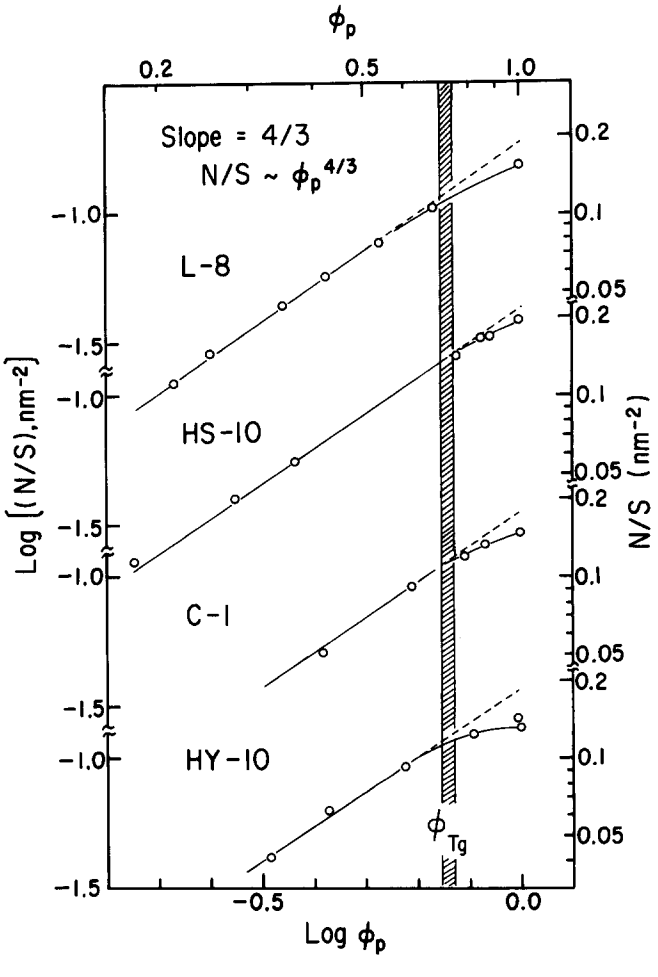

Figure 8 Change of interfacial density of the chemical junctions N/S with polymer concentrations ϕ_p for lamellar (L-8 and HS-10) and cylindrical microdomains (C-1 and HY-10). Straight lines show the change of N/S according to the scaling law $N/S \sim \phi_p^{4/3}$ relevant to the equilibrium regime. The deviation of the data points (open circles) from the straight line is due to the non-equilibrium effect

For lamellar domains N/S is determined by[9]:

$$N/S = \frac{DCN_A/2M}{wC + (1-C)/d_S} \tag{13}$$

with

$$w = W_{PS}/d_{PS} + (1 - W_{PS})/d_{PI}$$

where D is lamellar identity period (equal to the sum of PS and PI lamellar thicknesses); W_K is the weight fraction of K-block chain (K = PS or PI); d_K and d_S are the mass densities of K polymer and solvent, respectively; C is the weight fraction of polymer in solution, which is related to ϕ_p via:

$$\phi_p = \frac{wC}{wC + (1-C)/d_S} \tag{14}$$

M is the total molecular weight of the block polymer; and N_A is Avogadro's number. For cylindrical domains N/S is determined by[9]:

$$N/S = \frac{(\sqrt{3}/2\pi)^{1/2} DCN_A/2M}{[wC + (1-C)/d_S][(W_{PS}/d_{PS})/w]^{1/2}} \tag{15}$$

It is seen in *Figure 8* that the concentration dependences of N/S follow the scaling law relevant to systems in thermal equilibrium and given by equation (11) at $\phi_p < \phi_{T_g}$. However, at $\phi_p > \phi_{T_g}$, N/S values are smaller than those predicted by the scaling law, implying that the densification of the chemical junctions at the interface with increasing ϕ_p is suppressed by the non-equilibrium effect, as discussed above. The deviation from the scaling law becomes remarkable at $\phi_p > \phi_{T_g}$, indicating that the *vitrification* of one kind of microdomain is an important source of the non-equilibrium effects. However, one should note here the following two points: (i) even at $\phi_p > \phi_{T_g}$, i.e. even after the domain having higher T_g has attained vitrification, N/S still tends to increase with ϕ_p; and (ii) for some block polymers, e.g. L-8 and HY-10,

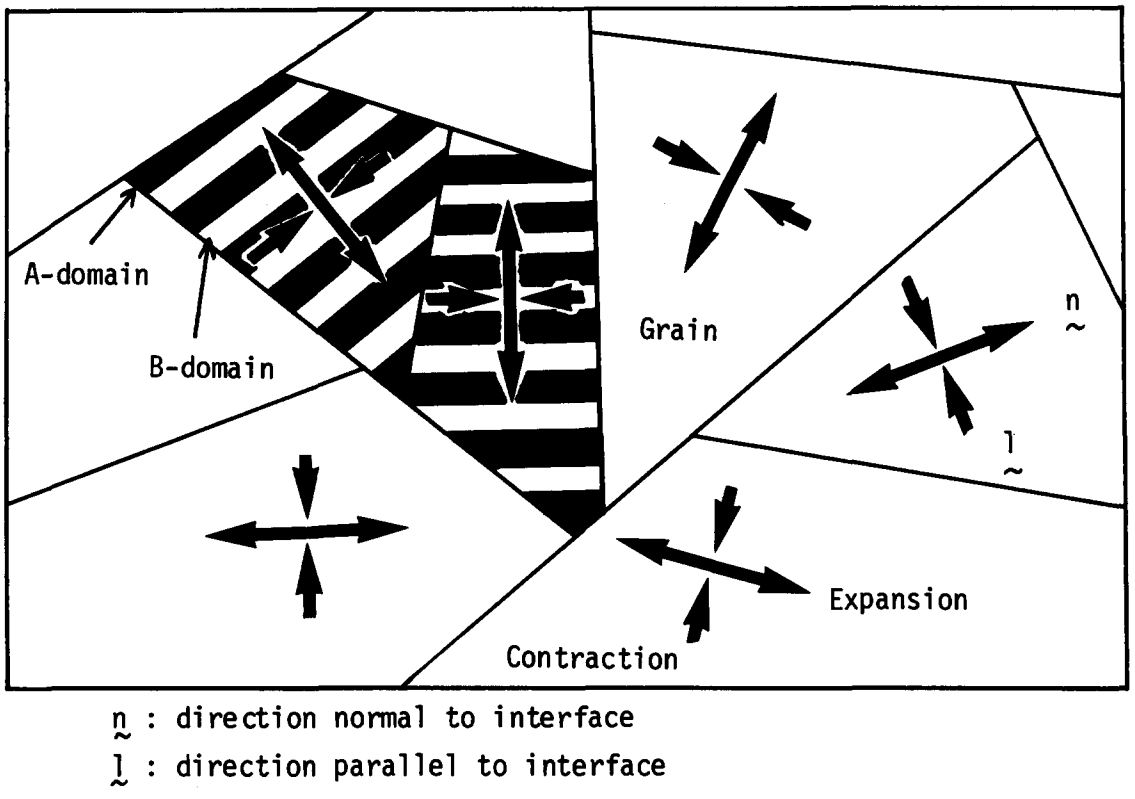

Figure 9 Grain-boundary relaxation as a possible non-equilibrium effect for lamellar and cylindrical microdomains. When segregation power increases, the grains expand and contract parallel to n and l, respectively. This process must involve cooperative deformation of the grains with characteristic relaxation time τ_{gr}. If the timescale of observation is shorter than τ_{gr}, the non-equilibrium effect on domain growth sets in even below the vitrification concentration ϕ_{T_g} or above the vitrification temperature T_g

the deviation from the scaling law and therefore the suppression of the densification of the chemical junctions at the interface occur at $\phi_p < \phi_{T_g}$ (see also *Figure 2*).

The observation specified in point (i) may happen because the timescale of the observations that allow us to determine N/S is extremely long, so that N/S can change even in the glassy state. This is a unique physical ageing effect in microdomain systems. It may happen also because the timescale of the observations on T_g is relatively short. If the cooling rate in the d.s.c. measurements is lowered, the measured T_g will be lowered and hence ϕ_{T_g} becomes higher. Point (ii) implies that the non-equilibrium effect may set in before the vitrification of one type of microdomain, even in the long timescale of the observations for N/S, and that there may be some mechanisms other than or in addition to vitrification that cause the non-equilibrium effect. One possible mechanism, which is called here *grain boundary relaxation* with relaxation time τ_{gr}, is sketched in *Figure 9*.

At high ϕ_p in *Figure 8*, the solution is space-filled with either lamellar (L-8 and HS-10) or cylindrical microdomains (C-1 and HY-10). However, the microdomains do not have perfect orientation. They rather have a 'grain' structure in which the orientation of the domains is correlated and specified by a director n, which is a unit vector parallel to the direction normal to the interface of lamellar microdomains or cylindrical microdomains. The orientation of the grains is macroscopically random, and hence n is also random. The diagram in *Figure 9* is simplified and as a consequence it looks as if there are grain-boundary walls where the mismatches of the microphases occur. However, in reality, the existence of such domain walls may be unfavoured as it causes excess interaction energy between PS and PI; rather, the domain

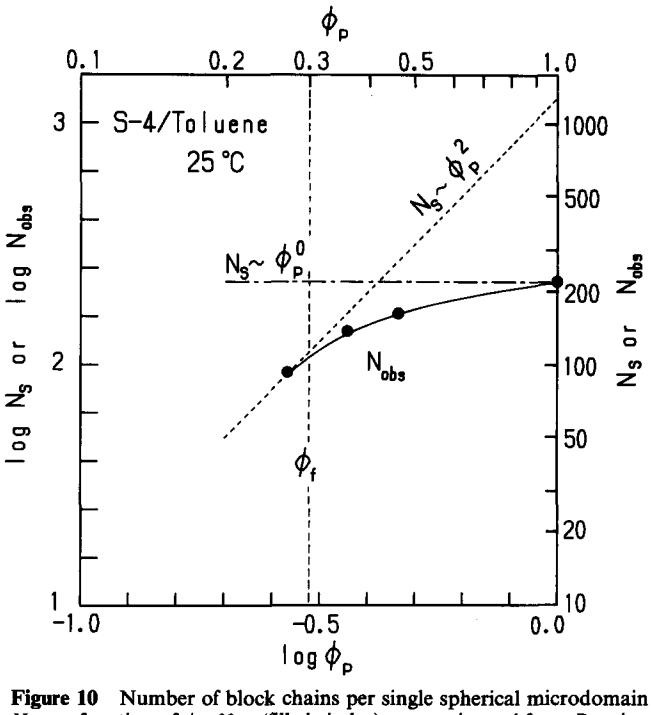

Figure 10 Number of block chains per single spherical microdomain N_s as a function of ϕ_p. N_{obs} (filled circles) were estimated from D_s using equations (16) and (17), b.c.c. lattice being assumed. The scaling law given by $N_s \sim \phi_p^2$ is for systems that attain thermal equilibrium, and that given by $N_s \sim \phi_p^0$ is for systems that cannot attain thermal equilibrium

orientation changes more or less continuously around the *disclinations* in a manner reminiscent to the texture of *nematic liquid crystals*.

The increasing segregation power with increasing ϕ_p causes expansion of the grain parallel to n and contraction

parallel to l, the unit vector parallel to the interface as shown by the arrows in *Figure 9*. The deformation of the grains driven by fundamental molecular rearrangements as shown in *Figure 7* cannot occur independently of one another but should occur cooperatively with other grains with a characteristic time τ_{gr}. If the timescale of observations on N/S or D (τ_{obs}) is shorter than τ_{gr}, the *grain-boundary relaxation time*, the non-equilibrium effect will set in even at $\phi_p < \phi_{Tg}$.

Therefore, we conclude that if $\tau_{obs} < \tau_{gr}$, the non-equilibrium effect is controlled by the grain-boundary effect; but if $\tau_{obs} > \tau_{gr}$, it is controlled by the vitrification effect.

Non-equilibrium process for systems with discontinuous interfaces

The number of block chains per single sphere, N_s, was determined from the experimental results of D_s using the following equation[9]:

$$N_s = \frac{CN_A a_c^3/kM}{wC + (1-C)/d_S} \tag{16}$$

with w as defined below equation (13), where a_c is the cell edge of the cubic system and is related to D_s by:

$$a_c = \sqrt{k}\, D_s \tag{17}$$

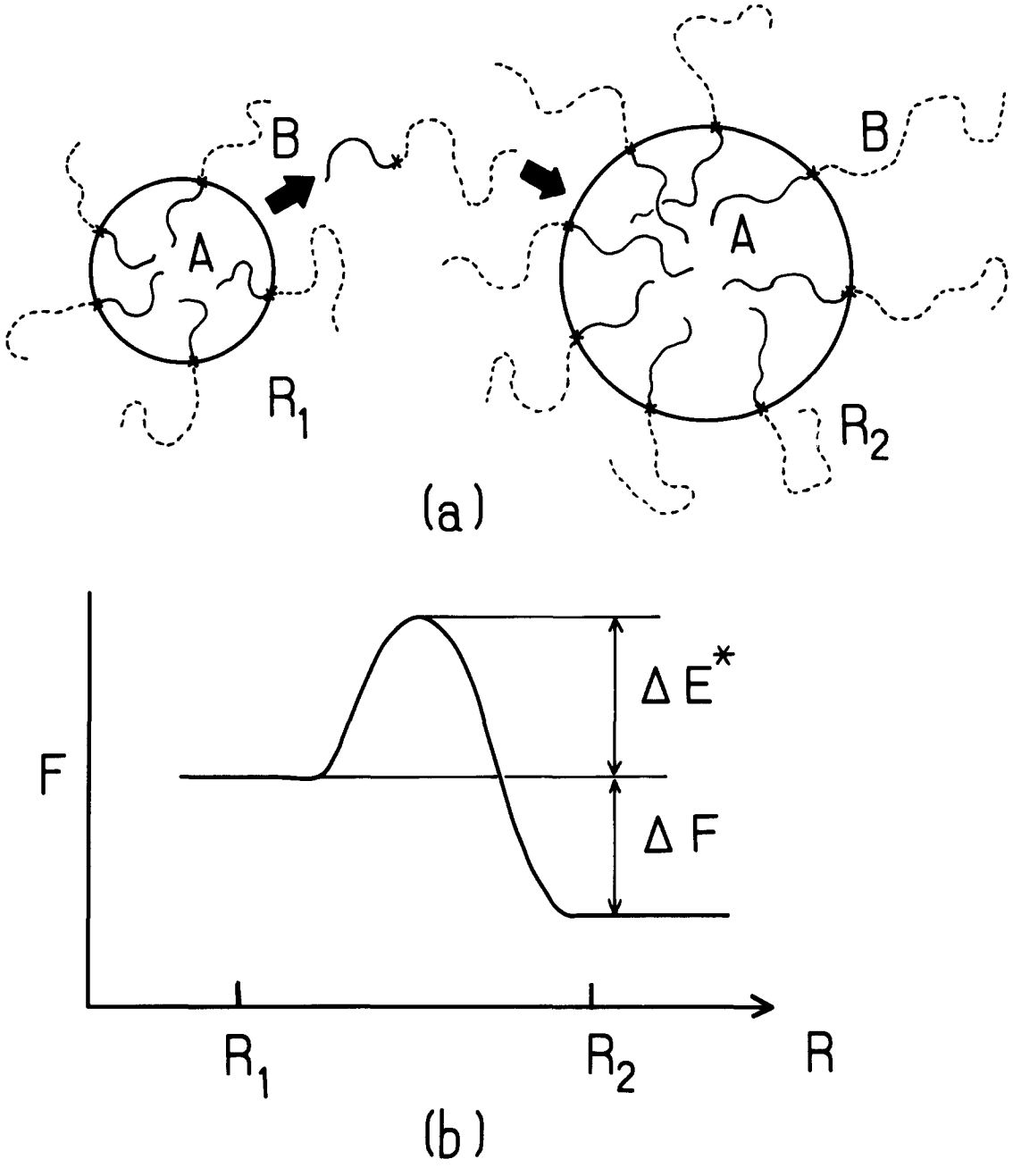

Figure 11 Sketch showing suppressed mutual diffusivity of the A–B diblock polymers forming spherical microdomains. (a) A possible molecular process causing domain growth. (b) ΔF and ΔE^* are, respectively, the free-energy difference between smaller and larger spheres and the potential barrier for mutual diffusion, which causes domain growth. $\Delta E^* \sim \chi_{eff} N$, where χ_{eff} is the effective Flory interaction between A and B monomers in the presence of the solvent, which increases with increasing ϕ_p, and N is the polymerization index for A–B block polymer. Note that for systems with continuous interfaces, such as lamellar and cylindrical domains, mutual diffusion takes place along the interface without involving the excess interaction ΔE^* between A and B

where k is a constant related to the symmetry of the cubic system, i.e. $k=1$, 2 and 3 for simple cubic (s.c.), body-centred cubic (b.c.c.) and face-centred cubic (f.c.c.) systems, respectively. The value of N_s thus estimated from D_s was defined as N_{obs} in *Figure 10*, where the b.c.c. lattice[5] was assumed. The figure also includes the concentration dependences of N_s in the cases when the system attains thermal equilibrium (equation (12)) and when the system completely fails to attain thermal equilibrium, i.e. $N_s \sim \phi_p^0$.

It is clear from *Figure 10* that the non-equilibrium effect for spherical microdomains sets in at $\phi_p = \phi_f \simeq 0.3$, a concentration much lower than those for lamellar and cylindrical microdomains. The solution with $\phi_p = 0.27$ was found to follow equilibrium closely from the experimental evidence that SAXS profile changed reversibly with temperature[5]. Thus for spherical systems:

$$\phi_f \ll \phi_{GB} < \phi_{T_g} \tag{18}$$

where ϕ_{GB} is the concentration above which the non-equilibrium effect due to the grain-boundary deformation becomes important.

The enhanced non-equilibrium effect in spherical microdomains is due to *suppressed mutual diffusivity* of block polymer chains at higher ϕ_p. If there is a thermodynamic driving force for the domain to grow, the average domain size grows from R_1 to R_2 as depicted in *Figure 11*. This growth, however, is inevitably accompanied by mutual diffusion of the block chain A–B in the matrix of B-rich solution according to the following stochastic path: evaporation of an A–B block chain from a spherical domain, translational diffusion of this A–B chain in the B-rich matrix over a distance, and condensation of the A–B chain into the same or another spherical domain. This mutual diffusion causes a penalty of unfavourable energetic interaction ΔE^* between A and B in the presence of commonly good solvent. This ΔE^* is an energetic barrier for mutual diffusion and hence domain growth, and is an increasing function of ϕ_p as:

$$\Delta E^* \sim \chi_{eff} N \tag{19}$$

and as the effective interaction χ_{eff} between A and B monomers in the presence of the solvent increases with increasing ϕ_p. In the mean-field approximation:

$$\chi_{eff} = \chi \phi_p \tag{20}$$

where χ is the bare interaction between A and B monomers. In (19), N is the degree of polymerization of A–B block polymer. When ϕ_p is increased, ΔE^* is hardly overcome by the thermal energy $k_B T$. Then the mutual diffusivity goes essentially to zero due to the thermodynamic factor, as discussed above.

Domain growth occurs as a consequence of mutual diffusion through the following molecular mechanisms: (i) the dissociation of A–B block chains from spheres with size R_1 and reassociation of these chains into spheres with size R_2 after mutual diffusion as shown in *Figure 11a* and discussed above, and (ii) the diffusion–coalescence of the smaller spheres into bigger spheres. The latter process (ii) involves the translational diffusion of the centre of mass of the spheres through the dissociation of A–B block chains from given spheres and reassociation of these chains in the same spheres after translational diffusion over a certain distance. As a result of such stochastic diffusion of the spheres, some spheres come sufficiently close to each other and coalescence into bigger spheres if they overcome the potential barrier exerted by the entropic repulsion of B-block chains emanating from the spheres.

ACKNOWLEDGEMENTS

The authors thank Professor D. J. Meier, Michigan Molecular Institute, Midland, MI, USA, for stimulating discussions during the course of this work. The authors gratefully acknowledge the financial support by a Grant-in-Aid for Scientific Research on Priority Area (63604558) from the Ministry of Education, Science and Culture, Japan, and by a grant from the Mitsubishi Foundation.

REFERENCES

1 Shibayama, M., Hashimoto, T. and Kawai, H. *Macromolecules* 1983, **16**, 16
2 Hashimoto, T., Shibayama, M., Kawai, H., Watanabe, H. and Kotaka, T. *Macromolecules* 1983, **16**, 361
3 Shibayama, M., Hashimoto, T., Hasegawa, H. and Kawai, H. *Macromolecules* 1983, **16**, 1427
4 Hashimoto, T., Shibayama, M. and Kawai, H. *Macromolecules* 1983, **16**, 1093
5 Shibayama, M., Hashimoto, T. and Kawai, H. *Macromolecules* 1983, **16**, 1434
6 Hasegawa, H., Tanaka, H., Yamasaki, K. and Hashimoto, T. *Macromolecules* 1987, **20**, 1651
7 Thomas, E. L., Alaward, D. B., Kinning, D. J., Martin, D. C., Handlin, D. L. Jr and Fetters, L. J. *Macromolecules* 1986, **19**, 2197
8 Hashimoto, T., Tanaka, H. and Hasegawa, H. *Macromolecules* 1985, **18**, 1864
9 Sadron, C. and Gallot, B. *Makromol. Chem.* 1973, **164**, 301